Equation (5) is a simple rearrangement of Eq. (4). Equation (6) follows directly from Eq. (5), in view of Jahnke–Emde,[5] pp. 149, 128, and 144, in that order.

More rapid convergence is obtained for small values of h by use of a Bessel product series:

$$b_1 = e^{-x^2-\frac{1}{2}h^2}\frac{1}{\pi}\int_{-\pi}^{x} e^{-2xh\sin\phi} e^{h^2\cos 2\phi}\sin\phi d\phi, \tag{7}$$

$$= 2e^{-x^2-\frac{1}{2}h^2}\sum_{n=-\infty}^{\infty} i^{-(n+1)}\bar{J}_n(\tfrac{1}{2}ih^2)J_{2n-1}(2ihx). \tag{8}$$

The exponential function of ϕ of Eq. (4) may be recognized as the generating function for Hermite polynomials,[6] hence Eq. (4) may be written:

$$b_1 = -he^{-x^2}\sum_{n=0}^{\infty}\left(\frac{h}{2}\right)^{2n}\frac{1}{n!(n+1)!}H_{2n+1}(x). \tag{9}$$

From the recursion relationships for Hermite polynomials,[6] we have:

$$b_1 = -hxe^{-x^2}\sum_{n=0}^{\infty} h^{2n}B_n, \tag{10}$$

$$B_0 = 2,$$

$$B_1 = x^2 - \tfrac{3}{2},$$

$$B_n = \frac{1}{2n(n+1)}\left[(2x^2+1-4n)B_{n-1} - \frac{2n-1}{n}B_{n-2}\right],$$

$$\left(\frac{\partial b_1}{\partial x}\right)_h = he^{-x^2}\sum_{n=0}^{\infty} h^{2n}B_n', \tag{11}$$

$$B_n' = \frac{1}{2^{2n}n!(n+1)!}H_{2n+2}(x),$$

$$B_0' = 4x^2 - 2,$$

$$B_1' = 2x^4 - 6x^2 + \tfrac{3}{2},$$

$$B_n' = \frac{1}{2n(n+1)}\left[(2x^2-1-4n)B_{n-1}' - \frac{2n-1}{n-1}B_{n-2}'\right].$$

The numerical values in Table I were primarily obtained by hand computation using Eqs. (10) and (11), as this is the simplest procedure in the absence of suitable tables of modified Bessel functions. In practice, h is generally small and two to six terms will suffice. At $h=2.4$, the most difficult hand computation attempted, sixteen terms were required for four-place accuracy, twenty terms for seven places. We wish to acknowledge the kindness of the Friden Company for the loan of a desk calculator to check some of the more involved computations.

For the Fourier coefficients, in general, we have $a_{2k+1}=b_{2k}=0$, as proved earlier.[2] For the cosine coefficients:

$$a_0 = e^{-x^2}\sum_{n=0}^{\infty}(h/2)^{2n}(n!n!)^{-1}H_{2n}(x), \tag{12}$$

$$a_{2k} = (-1)^k 2e^{-x^2}\sum_{n=0}^{\infty}(h/2)^{2n+2k}(n!(n+2k)!)^{-1}H_{2n+2k}(x), \tag{13}$$

and for the sine coefficients:

$$b_{2k+1} = (-1)^{k+1}2e^{-x^2}\sum_{n=0}^{\infty}(h/2)^{2n+2k+1}(n!(n+2k+1)!)^{-1}H_{2n+2k+1}(x). \tag{14}$$

The possibility has been investigated, without success, that the derivative extremum at the modulation frequency, defined by the nontrivial solution of

$$(\partial b_1/\partial x)_{h,x=x_0} = 0,$$

might have a simple, closed-form solution. The limiting value of x_0, as h approaches zero, is $\frac{1}{2}\sqrt{2}$. A remarkably close approximation to x_0, for small values of h, is given by

$$H_2(x_0) = 4x_0^2 - 2 \doteq h^{-2}(\cosh\sqrt{2}h - 1)^2 \quad (h \lesssim 1). \tag{15}$$

The error associated with Eq. (15) increases rapidly as h goes above unity: The calculated value for x_0 from Eq. (15) is low by 0.02% at $h=0.8$, too high by 0.07% at $h=1$, but too high by 0.60% at $h=1.2$. For larger values of h a graph of $(x_0^2-\frac{1}{2})^{\frac{1}{2}}$ vs h seems to approach the asymptote:

$$(x_0^2-\tfrac{1}{2})^{\frac{1}{2}} \doteq h - \tfrac{1}{2} \quad (h \gg 1). \tag{16}$$

(With the present normalization procedure,[2] it seems worth mention that the simple, closed-form solution for a Lorentzian line shape,[3] is

$$3x_0^2 = 5 + 3h^2 - 2(4+3h^2)^{\frac{1}{2}}, \tag{17}$$

from which it is an easy matter to compute the measurement broadening.)

The peak value of $|b_1|$ is 0.574411_5. This occurs at $h=1.3179_5$ and $x_0=1.1082_4$. For larger values of h the peak derivative amplitude slowly diminishes and an inflection appears in the derivative record, in a manner analogous to that for a Lorentz curve above $h=2.00$ (with Lorentz normalization), for which $|b_1|_{\max}=0.50$ and $x_0=\sqrt{3}$.[7]

* Present address: Aerospace Engineering Department, University of Florida, Gainesville, Florida.

[1] G. W. Smith, J. Appl. Phys. 35, 1217 (1964).
[2] O. E. Myers and E. J. Putzer, J. Appl. Phys. 30, 1987 (1959).
[3] H. Wahlquist, J. Chem. Phys. 35, 1708 (1961).
[4] G. V. H. Wilson, J. Appl. Phys. 34, 3276 (1963).
[5] E. Jahnke and F. Emde, *Tables of Functions* (Dover Publishing Company, New York, 1945).
[6] P. M. Morse and H. Feshbach, *Methods of Theoretical Physics* (McGraw-Hill Book Company, Inc., New York, 1953), Part 1, p. 768. There is a misprint on this page: the formula should read:

$$(d/dz)[e^{-z^2}H_n(z)] = -e^{-z^2}H_{n+1}(z).$$

[7] O. E. Myers, Convair Sci. Res. Lab. Rept. 3 (June 1958); Fig. 10, with acknowledgment to E. J. Putzer.

Laser-Stimulated Nucleation in a Bubble Chamber*

R. C. Stamberg and D. E. Gillespie
Department of Nuclear Engineering, The University of Michigan, Ann Arbor, Michigan

(Received 15 March 1965; in final form 16 August 1965)

It has been found that bubble chambers can be made sensitive to nucleation stimulated by a pulsed ruby laser with output at 6943 Å. A 6-in.-diam bubble chamber containing $CBrF_3$ (Freon) at 30.7°C was used with a 6% free volume before compression. The chamber was more sensitive to laser-stimulated nucleation than radioactive-stimulated nucleation from a powerful gamma ray source. Shadow photographs showed that the threshold for nucleation from the laser beam occurred below 0.2 mJ/cm² while increases in the energy of the laser beam to 25 mJ/cm² caused a greater number of bubbles to form, using a constant superheat condition. The bubbles reached visible size 50 msec after the laser beam entered the chamber. The formation of bubbles was apparently caused in the superheated bubble chamber by the absorption of a large number of photons from the laser beam onto a trace of minute particles (mostly dust) floating in the liquid Freon. A "hot" particle then caused bubbles to nucleate and the superheat in the chamber caused the bubbles to grow.

The interaction between intense light and matter during nucleation or cavitation in a liquid creates unusual effects. The pressure increase associated with the collapse of bubbles can release part of the energy as visible light when nuclei such as microscopic dust particles or other contaminants are present.[1] The reverse process is also possible. The light beam from a pulsed laser at 6943 Å produces nucleation when a superheated liquid is created by the appropriate pressure drop. With a superheated

liquid, the minimum energy flux necessary for the first bubbles to form in a bubble chamber is below 0.2 mJ/cm² during a 600-μsec period. The laser beam enters the 6-in.-diam bubble chamber used for this report with a 2.0-cm² cross-sectional area. The particles in the chamber were essentially dust trapped before the chamber was filled with pure distilled Freon which had been filtered through a 40–50 μ sintered metal filter.

The formation of bubbles in a pure liquid does not, however, require the presence of foreign solids in the chamber since bubbles have been observed in a pure, colorless liquid such as water or benzene.[2] This was accomplished by focusing the beam from a giant (Q-switched) ruby laser into a container assumed to be at 1 atm. Bubble formation in this case was caused by forcing the dielectric breakdown of the fluid into a "plasma." Maximum power inputs of 42 W/cm² (for an energy flux of 25 mJ/cm²) into the bubble chamber were about 10^{-5} those from Q-switching.

Nucleation in the 6-in.-diam chamber was recorded as a series of photographs taken after the bubbles first became visible at a diameter of 0.5 mm (Fig. 1). This occurred about 50 msec after the laser beam entered the chamber. Figure 2 is a typical photograph taken 100 msec after the laser beam with an energy flux of 12 mJ/cm² entered the chamber having a pressure drop of much less than 160 psi from an initial pressure of about 310 psig. The number of bubbles were repeatable within about 10% using constant, controlled conditions. The error was primarily due to randomness of nucleation sites. The number of bubbles is a function of the laser beam energy, using a constant superheat condition. The size of each bubble is essentially determined by the length of the time elapsing after the laser beam initially enters the chamber until the photograph is taken.

A greater degree of sensitivity to laser-stimulated nucleation rather than radioactive-stimulated nucleation was shown by using two bubble chambers. In a 40-in.-diam chamber, built by the Physics Department at The University of Michigan for Argonne National Laboratory, a 0.5-mCi ^{60}Co source induced nucleation very easily. Many thousands of bubbles formed in this large chamber using the same conditions of $CBrF_3$ at 30.7°C with a 6% free volume before compression and an expansion from 310 psig. The 6-in.-diam chamber, on the other hand, was not sensitive to the ^{60}Co source, but very sensitive to laser-stimulated nucleation. This is caused by a much smaller degree of superheat in the 6-in. chamber than the 40-in. chamber. A pressure drop of about 160 psi in the 40-in. chamber is sufficient to cause radioactive-stimulated nucleation, while a pressure drop of less than 160 psi in the 6-in. chamber is sufficient to cause only laser-stimulated nucleation.

Laser stimulated nucleation in a bubble chamber is a relatively simple process. The laser beam enters into the superheated liquid where the beam deposits part of the energy onto very small dust particles, assumed to have a maximum diameter of about 0.2 mm and a concentration of about 1/cm³ floating randomly in the Freon. Some particles then become so "hot" that they boil the Freon surrounding them to form microscopic bubbles which then grow using the superheat in the chamber. The result is a random assortment of bubbles anywhere the beam first traversed the chamber. A concave mirror, opposite the location where the beam entered the chamber, spreads the beam so that is can't cause nucleation on dust particles after reflecting more than two inches from the mirror.

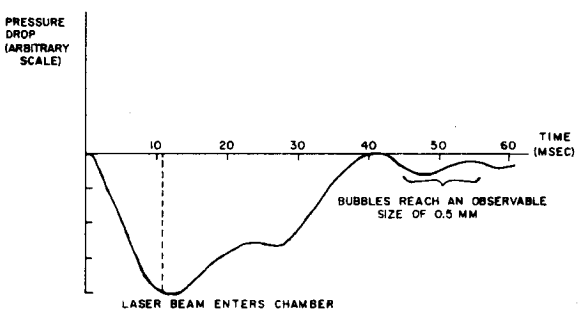

FIG. 1. Sequence of events in a 6-in.-diam bubble chamber relative to pressure versus time. The curve was obtained using an Endevco transducer on the side of the bubble chamber.

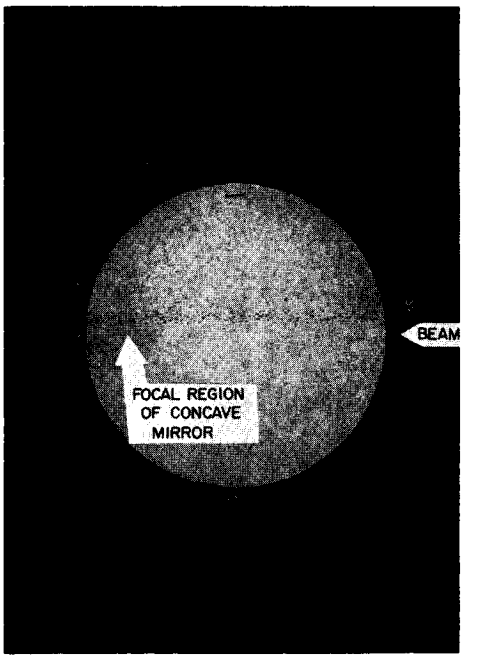

FIG. 2. Laser stimulated nucleation in a 6-in.-diam bubble chamber. Photograph taken 100 msec after a ruby laser beam with an energy flux of 12 mJ/cm² entered the chamber.

To demonstrate that dust particles in the chamber must be the nucleation sites, we first prove that the colorless Freon is not responsible for the bubble nucleation. Experimental results show that the number of bubbles increases as the energy of the laser beam increases when we consider the total volume traversed by the laser beam in the chamber. If we assume a completely uniform material in the bubble chamber down to molecular dimensions, then, a much greater light intensity focused on a small volume of the total volume should produce a larger number of bubbles than is produced where the intensity of the beam is lower. The focal "point" (or region) of the concave mirror in the chamber represents the small volume increment. The focal region has a greater light intensity than the unfocused beam by a factor of 200. However, the photographs taken at the threshold of nucleation, which show only about three bubbles, indicate no greater concentration of bubbles in the focal region. We conclude that the material causing the bubbles is not uniformly dissolved in the Freon. The small, undissolved material is probably particles distributed randomly in the chamber. This conclusion can be verified without a camera by observing a dust particle by eye and noting that bubbles grow from that "point" after it is illuminated by the laser beam. Final proof presumably could be obtained by changing the concentration of particles to observe a correspondingly different number of bubbles, holding all other conditions constant; although this has not been attempted.

We can conclude that the lint and dust particles which absorb light at 6943 Å are the source of nucleation. It is reasonable to conclude that the $CBrF_3$ absorbs negligible light since $CBrF_3$ has shown no significant absorption at 6943 Å.[3]

A comparison of relative energy values helps to indicate how energy absorbs on dust. Bugg[4] determined that the kinetic energy

associated with the growing bubbles in a superheated liquid had a minimum value of 18.4 eV while the photons of the laser beam have an energy of only 1.78 eV. This requires that at least 11 photons absorb onto a nucleation site. However, assuming that each site occupies 10^{-4} of the cross sectional area of the beam entering the chamber, a total of about 8×10^{12} photons (for a 12 mJ/cm² ruby laser beam) would absorb on, reflect off, or transmit through a nucleation site of a dust particle. This substantiates simply that the intensity of the laser beam is large enough to deposit sufficient energy on the particles to cause boiling at the nucleation sites.

Paths of bubbles up to 1 cm long are observed on the photographs. This may indicate that during nucleation the heated dust particles in the chamber tend to diffuse in the direction of the laser beam, i.e., the particles tend to move away from their hot side.

The authors express deep gratitutde to Professor Chihiro Kikuchi, Department of Nuclear Engineering, The University of Michigan, for his appreciation of this work and encouragement. The authors also appreciate the helpful advice received from Professor Osborn, also in this department, and Professor Vander-Velde of the Physics Department.

* This work was supported in part by grants from the National Science Foundation and National Aeronautics and Space Administration.

[1] P. D. Jarman and K. J. Taylor, Brit. J. Appl. Phys. **15**, 321 (1964).
[2] R. G. Brewer and K. E. Rieckhoff, Phys. Rev. Letters **13**, 334 (1964).
[3] Thomas M. Dunn (private communication).
[4] D. V. Bugg, Progr. Nucl. Phys. **7**, 13 (1959).

Surface and Interface Waves in Plasma Gaps*

C. DAVIS
RCA Laboratories, Princeton, New Jersey
AND
T. TAMIR
Electrophysics Department, Polytechnic Institute of Brooklyn, New York
(Received 29 March 1965)

THE presence of a low-density sheath at the interface between a rigid surface and a neutral plasma medium has attracted considerable attention lately. Such a sheath may appear at the walls of a receptacle containing a plasma discharge or around the structure of a missile moving in the ionosphere. In most cases, the situation is that of a gap, sparsely filled with ions and electrons, which separates a conducting or isolating boundary from an electrically neutral, ionized, gas with highly mobile electrons.

The purpose of this note is to examine the waveguiding properties of the boundary interface produced by a gap in a plasma medium. In particular, it is found that interface waves which are tightly bound to that boundary may occur; some of these waves show pronounced backward-wave characteristics which may be responsible for certain instabilities in the plasma medium. The interesting feature of the backward waves discussed here is that they occur when a small gap is associated with a *thick* plasma layer.[1] Previous investigations[2-4] have shown that the backward-wave character usually appears in the presence of *thin* plasma layers and the present work therefore suggests that backward waves may occur under conditions which are substantially different from those known hitherto.

To simplify the discussion, a planar geometry is assumed wherein a gap exists in an unbounded plasma environment. The plasma medium itself would normally occur in the form of a layer; however, since one looks for waves which decay away from the interface at the gap, the thickness of the plasma layer would have little effect if one excludes the possibility of very thin layers. Hence the geometry of the gap is well approximated by the configuration shown in Fig. 1. To further simplify this model, it is assumed that the medium in the gap is characterized by the permeability μ_0 and the permittivity ϵ_0 of vacuum, i.e., the presence of the relatively few electrons and ions in the gap is neglected when compared with the effect of the numerous electrons and ions in the

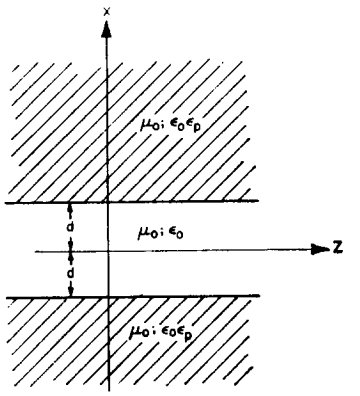

FIG. 1. Geometry of the plasma gap.

plasma medium. Furthermore, the gap is assumed to be well defined by sharp plasma–vacuum interfaces at $x=\pm d$ and the plasma medium is taken to be homogeneous, isotropic, and lossless; if it is assumed that the positive ions are stationary and the thermal motion of electrons is disregarded, the plasma region is characterized by a relative dielectric constant:

$$\epsilon_p=1-(\omega_p/\omega)^2. \tag{1}$$

The configuration was already investigated by Lichtenberg and Woodyard[5] who assumed, however, that an infinite magnetic field was present in the z direction. A similar planar structure was examined by Oliner and Tamir[2] who considered a geometry like that of Fig. 1, but with the plasma and vacuum regions interchanged.

To render the problem two-dimensional, we shall look for waves which are invariant with respect to the y direction ($\partial/\partial y\equiv0$) and propagate along the z direction as $\exp[i(k_z z-\omega t)]$. It is then readily verified that the fields are separable into the familiar E and H modes. The symmetry with respect to the yz plane simplifies the analysis by considering two separate and simpler cases: (a) in the first, the yz bisecting plane is taken as a perfect electric conductor which corresponds to a short-circuit bisection and is denoted as the (sb) case; (b) in the other case, the yz bisecting plane is taken as a perfect magnetic conductor which corresponds to an open-circuit bisection denoted as the (ob) case. It is recognized that the short-circuit (sb) case yields waves which occur at the gap between a plasma layer and a metallic wall; the open-circuit (ob) case is more appropriate for gaps produced by dielectric sheets which are introduced into a plasma medium.

Let us designate the transverse wavenumber (in the x direction) by k_x in the gap region and k_{xe} in the plasma regions. Using conventional methods, the secular equations are easily obtained via Maxwell's equations which yield:

$$\begin{matrix} H\ modes & & E\ modes \end{matrix}$$
$$i\frac{k_{xe}}{k_x}=\begin{cases}\cot k_x d & \text{(sb)}\\ -\tan k_x d & \text{(ob)}\end{cases} \qquad i\frac{k_{xe}}{\epsilon_p k_x}=\begin{cases}-\tan k_x d & \text{(sb)}\\ \cot k_x d & \text{(ob)}\end{cases} \tag{2}$$

where the various wavenumbers are related by

$$k_x^2+k_z^2=k^2, \tag{3}$$

$$k_{xe}^2+k_z^2=k^2\epsilon_p; \tag{4}$$

with $k^2=\omega^2\mu_0\epsilon_0$. By subtracting (4) from (3), one has

$$(k_x d)^2-(k_{xe}d)^2=(kd)^2(1-\epsilon_p)=\left(\frac{\omega_p d}{c}\right)^2=\left(2\pi\frac{d}{\lambda_p}\right)^2=b^2, \tag{5}$$

where $c=\omega_p\lambda_p/2\pi$ is the speed of light in vacuum. Hence b appears as a dimensionless parameter, which is characteristic of the problem since it involves both the geometry (via the half-spacing d) and the physical state of the medium (as given by λ_p). Clearly, small and large values of b refer to narrow and wide gaps, respectively.

The guided waves considered here are assumed to propagate